ISSN 1560-0904, Polymer Science, Series B, 2020, Vol. 62, No. 6, pp. 612–620. © Pleiades Publishing, Ltd., 2020.

CATALYSIS

Reactor Blend and Nanocomposite of Polyethylene Using a Binary Catalyst of Metallocene/Nickel

Mohammad Kazemi[a], Ali Javidnia[a], Navid Ramezanian[a,*], Gholam Hossein Zohuri[a], and Mohsen Mogheiseh[a]

[a] *Department of Chemistry, Faculty of Science, Ferdowsi University of Mashhad, Mashhad, 91775-1436 Iran*

**e-mail: ramezanian@um.ac.ir*

Received May 10, 2020; revised August 14, 2020; accepted August 23, 2020

Abstract—The present study aimed to conduct the ethylene polymerization using two binary catalytic systems to evaluate the resulting reactor blend of polyethylene. Subsequently, the study continued to explore the effects of catalyst to monomer molar ratio, reaction temperature, ethylene pressure and nanofillers on the catalysts activity, molar mass, thermal behavior, structural and morphological properties of the obtained polyethylene. The catalytic system containing α-diimine catalyst based on nickel showed higher activity, higher melting point (75.6×10^4 g polyethylene/(mol catalyst h), 125°C, respectively) and the extent of crystallinity (up to 48.5%) in comparison with the analogous system bearing pyridine-imine catalyst. The augmentation of nanoparticles increased the branching content in the system with α-diimine catalyst based on nickel, while these trends were reverse in pyridine-imine catalyst system, so that the branches were reduced as the nanoparticle concentration was increased. SEM images revealed distinct fibrous phases and the presence of obvious and well dispersed nanoparticles in the prepared nanocomposites. The synthesized polyethylene blend exhibited high thermal stability.

DOI: 10.1134/S1560090420330027

INTRODUCTION

With the advent of metallocene catalysts in early 1980s, single site catalysts have attracted further attentions in olefin polymerization. These catalysts are well known for their excellent flexibility and versatility to control the polymerization reaction and significant bulk properties of the resulting polymers. These highly active single type catalysts are capable to produce polymers with narrow molecular weight distribution and chemical composition distribution [1, 2]. To produce a new family of advanced polyolefin material, interests have switched to late-transition metal complexes in both industrial and scientific researches. The beginning was through the discovery of α-diimine metal (nickel and palladium) and bis(imino)pyridyl metal (iron and cobalt) complexes reported in the middle of 1990-s for olefin polymerization [3, 4]. In comparison to metallocenes, the products derived from nickel complexes are highly branched even in the absence of α-olefin comonomer, whereas linear polyethylene (PE) was generally produced from catalyst systems based on iron or cobalt pre-catalysts [5–7]. Therefore, ethylene polymerization using combining the metallocene with nickel-based catalysts provides a new approach to produce a wide range of polyethylene grade from highly branched to a linear, and semi-crystalline and high-density materials [8, 9]. These structural properties of polyethylene can be adjusted during the original polymerization procedure by combining two or more types of catalysts inside a single reactor [10]. Basically, each catalysts produces polyethylene independently to form reactor blend. Thus, the final product properties may be achieved through simple adjustment of the catalysts ratio and polymerization conditions, as well. Combination of the catalysts to reach desired properties of final product can be achieved through three methods: a) injecting of second catalyst at a determined polymerization time, which can continue polymerization with or without deactivation of the first catalyst (transition method) [11, 12], b) introducing two different catalysts in regard to structure into the polymerization reactor simultaneously and independently (mixing method) [13, 14], and c) operating the polymerization with two catalysts loaded on a support (hybrid method). Besides to the techniques, choosing a proper catalyst structure to reach desired polymer properties is critical [15, 16].

Graphene as one of the special carbon allotropes has outstanding physicochemical properties with high optical transmittance, large surface area, high thermal/electrical conductivity and high mechanical properties, predisposing promising nanofiller for polymer nanocomposites [17, 19]. According to previ-

ous studies, the effectiveness of carbon nanotubes (CNTs) as filler in polymer mixture depends on both intrinsic properties of carbon nanotubes and their dispersion and alignment in composites [13, 20, 21], which is hard to achieve, especially in non-polar polymeric matrixes such as polyolefins. Therefore, a uniform dispersion of particles along with maintaining the unique properties of these materials is a challenge. In-situ polymerization is a promising technique to fabricate the polyolefin/nanocomposites [13, 14]. The current study reports the results of ethylene polymerization using combination of catalysts, followed by the evaluation of the effects of catalyst composition and polymerization conditions (such as co-catalyst concentration, monomer pressure, reaction temperature) on microstructure of linear/branched polyethylene in the reactor blends. Furthermore, the impact of the nanofiller type on catalytic behavior along with properties of the obtained PE/nanocomposites (such as thermal, morphological and microstructural) was studied.

EXPERIMENTAL

Materials and Methods

Polymerization-grade ethylene monomer (with purity of 99.9%) was purified and dried by passing through activated molecular sieve columns. Anhydrous toluene and non-halogenated solvents, including diethyl ether was refluxed over Na/benzophenone and distilled under ultra-pure argon atmosphere prior to use. Similar equipment was employed to purify dichloromethane, while CaH_2 was used as a drying agent. The pyridineimine and the α-diimine based on nickel (II) bromide complexes were synthesized in accordance to our previous reports [6, 22]. The catalysts precursor of zirconocene dichloride was purchased from Sigma Aldrich. Triisobutylaluminium was supplied from Sigma Aldrich Chemical, which was used to synthesize MMAO [23]. The MWCNTs with two different sizes and diameters (with outer diameters of 20–30 and 30–50 nm and specific surface area of 110 and 60 m^2/g, respectively) and graphene/nano-platelets (1.7–2.0 nm with 10–12 layers and specific surface area of 500–1200 m^2/g) were purchased from US research nanomaterials, which were utilized without any further purification. All experiments on air and/or moisture sensitive compounds were carried out under inert and dry atmosphere in a glove box.

General Procedure for Ethylene Polymerization

All polymerization processes were performed in a sealed glass reactor equipped with Schlenk system, ethylene inlet, mechanical stirrer, temperature and pressure controllers. The reactor was degassed and filled with ethylene several times for removal of oxygen and moisture. The MMAO as co-catalyst was injected into the reactor which containing toluene under the inert conditions. The polymerization was initiated by introducing the appropriate amount of catalyst(s) into the reactor. The total pressure was kept constant by a continuous feed of the ethylene gas. After venting the residue of monomer, the polymerization was quenched by acidified methanol (5% v/v). The resulting polyethylene was collected by filtration, washed several times with small portions of methanol and dried under the reduced pressure [13].

Procedures for Preparation of PE/Nanocomposites

Desired amount of different types of nanofiller suspension (in toluene) was added to a round bottom flask containing toluene for dissociation of the particles prior addition of the catalysts. The reactor was pressurized with ethylene up to 2 bars. At the end of polymerization, the reaction mixture was poured into an acidified methanol (5% v/v). The quenched solid was filtered and washed with methanol for further purification.

Characterization

FTIR spectra were recorded by Thermo Nicolet AVATAR 370 for determination of vinyl and branching content, which were calculated on the basis of literatures [6, 24]. The viscosity average molecular weight $\bar{M}_v$ of the polymer samples was determined according to the literature ($[\eta] = 6.2 \times 10^{-4} M_v^{0.7}$) [25]. Thermal gravimetric analysis (TGA) (Perkin Elmer TGA-7) and differential scanning calorimetry (DSC) instruments (Mettler Toledo DSC822) were used for characterization of the polyethylene and the nanocomposites at a constant rate of 10 grad/min. Degree of crystallinity of the samples was calculated on the base of its enthalpy of fusion, which was determined by DSC [26]. SEM images were recorded using LEO VP 1450 instrument.

RESULTS AND DISCUSSION

The polymerization was performed using two different binary catalyst systems, as shown in Scheme 1. As follows from our previous studies, the first catalytic system (**S_1**) included zirconocene (Z) and 2-[(2,6-diisopropylphenylimino)ethyl]pyridine nickel dibromide (N_p) catalysts and the second group (**S_2**) contained zirconocene and 1,4-bis(2,6-diisopropylphenyl) acenaphthenediimine nickel (II) dibromide (N_α) catalysts were mixed separately in the reaction media at equal ratio of the catalysts fraction (5 : 5 μmol). In the presence of MMAO as co-catalyst, effects of some parameters, including [Al]/[Ni] molar ratio, polymerization temperature and monomer pressure on catalytic activity, viscosity average molecular weight, melt-

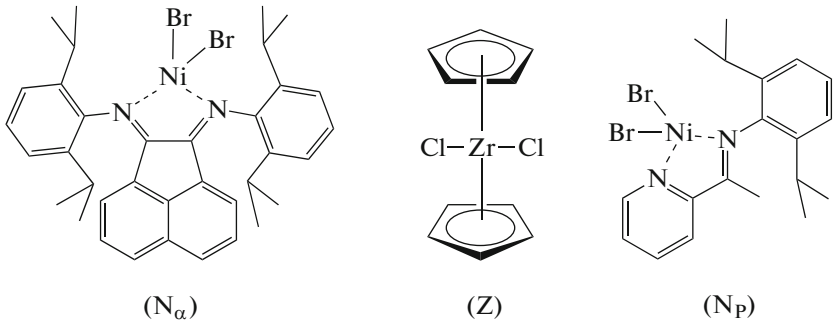

(N_α) (Z) (N_P)

Scheme 1.

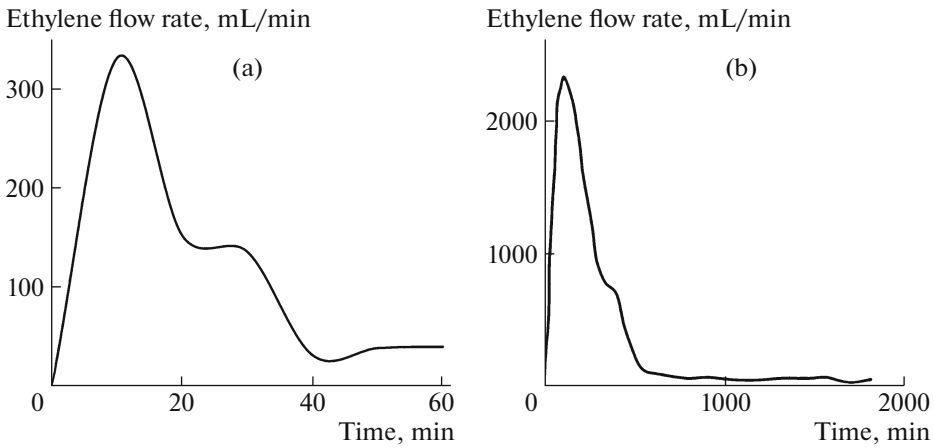

Fig. 1. Kinetic profile of ethylene polymerization using N/Z/MMAO binary system: (a) S_1, (b) S_2.

ing point, degree of crystallinity, vinyl and branching content (per 1000 carbon atoms) of resulting product were evaluated (Table 1).

The polymerization activity of both catalytic systems (S_1 and S_2) slightly increased as co-catalyst ratio raised from 500 to 1250 and reached to the highest values at the [Al]/[M] molar ratio of 1000 and 1250 for S_1 and S_2, respectively (Entries 4, 18, Table 1). This behavior may be attributed to formation of deactivated form of active site and lower activity of the catalysts during of the polymerization as the concentration of the co-catalyst goes higher than the optimum [27, 28]. The higher activity of N_α in the catalyst system (S_2) enhanced overall catalytic activity of the system and $\bar{M}_v$ compared with S_1 system. While, higher and effective lifetime of ethylene polymerization was observed for S_1 system (Fig. 1), which can be attributed to long lifetime of the catalyst N_p [6]. Influence of reaction temperature on the catalyst behavior was investigated in the range of −10 to 30°C (Entries 6–10, 14 and 19–22) at 2 bar of ethylene pressure. With raising the polymerization temperature, both catalytic activity and $\bar{M}_v$ of the obtained products first increased and reached an optimum value at 0°C with following decline, which could be ascribed by instability of active centers or even lower concentration of ethylene in the reaction media at higher temperatures [5, 22]. For S_2 catalytic system, as ethylene pressure augmented (Entries 17 and 23–25), both catalytic activity and $\bar{M}_v$ continuously increased. The similar trend was observed for S_1 catalytic system with a little difference. From 1 to 4 bar of ethylene pressure (Entries 4 and 11–13), the observed activity along with $\bar{M}_v$ of the resulting products slightly increased and reached the highest values at 2 bar (Entry 7). Further increasing of pressure up to 4 bar, however, lead to a slightly decrease in both activity and molecular weight of the resulting polyethylene blend. In fact, replacing the catalyst N_α into the catalyst combination (instead of catalyst N_p) led to more diffusion of ethylene to the active center and more possible chain termination than chain propagation [21, 29, 30].

Effect of type and content of nanoparticles was evaluated on both catalytic activity of S_1 and S_2. The polymerization was conducted in the presence of catalyst systems (equal molar ratio of the catalysts) at reaction temperature of 0°C and 2 bar of ethylene pressure for a determined period of time. Addition of

Table 1. Results of ethylene polymerization

Entry	Catalytic system	[Al]/[M]	T_p, °C	P, bar	Time, min	PE, g	Act.[a]	$\bar{M}_v$[b]	T_m[c], °C	X_C[c], %	VC[d]	BD[e]
1	N_p (10 μmol)	1000	0	2	60	3.62	18.2	0.9	103	30.4	5.26	68.9
2	S_1 (5 μmol N_p + 5 μmol Z)	500	0	1	60	2.34	23.4	n.d.	–	–	–	–
3		750	0	1	60	2.86	28.6	n.d.	–	–	–	–
4		1000	0	1	60	4.96	49.6	n.d.	–	–	–	–
5		1250	0	1	60	4.43	44.3	n.d.	–	–	–	–
6		1000	– 10	2	60	5.0	50.1	9.1	–	–	–	–
7		1000	0	2	60	5.39	53.9	8.2	83	26.8	2.85	–
8		1000	10	2	60	3.82	38.2	7.0	–	–	–	–
9		1000	20	2	60	2.71	27.1	3.1	–	–	–	–
10		1000	30	2	60	2.32	23.2	1.9	–	–	–	–
11		1000	0	1	60	4.72	47.2	8.0	–	–	–	–
12		1000	0	3	60	4.48	44.8	7.7	–	–	–	–
13		1000	0	4	60	4.25	42.5	7.6	93	27.5	–	–
14	Z (10 μmol)	1000	0	2	30	1.25	6.2	n.d.	135	96.1	–	–
15	S_2 (5 μmol N_α + 5 μmol Z)	500	0	2	30	2.45	49.0	n.d.	–	–	–	–
16		750	0	2	30	3.24	64.8	4.2	–	–	–	–
17		1000	0	2	30	3.78	75.6	4.4	125	20.1	0.90	32.3
18		1250	0	2	30	3.82	76.4	n.d.	–	–	–	–
19		750	– 10	2	30	2.11	42.2	n.d.	–	–	–	–
20		750	10	2	30	3.17	64.2	2.9	–	–	–	–
21		750	20	2	30	1.04	20.8	1.3	–	–	–	–
22		750	30	2	30	0.81	16.2	0.9	–	–	–	–
23		1000	0	1	30	1.94	38.8	3.9	–	–	–	–
24		1000	0	3	30	5.48	110	5.3	131	34.9	4.0	21.1
25		1000	0	4	30	5.91	118	n.d.	–	–	–	–
26[Rubber]		1000	20	2	20	1.34	26.8	1.9	113	12.3	41.30	12.0
27	N_α (10 μmol)	1000	0	1	30	1.70	33.4	1.2	110	28.5	–	–

[a] Activity, $\times 10^4$ g (PE) mol/(Ni+Zr) h.
[b] The viscosity average molecular weight, $\times 10^4$.
[c] Determined by DSC [26].
[d] Vinyl content: determined by FTIR [24], number of vinyl groups/1000 carbon atoms.
[e] Branching density: determined by FTIR [6], methyl branches/1000 carbon atoms.

the nanoparticles during polymerization caused a decreasing of activities for both catalyst combinations (Table 2). The observed trend might be due to deactivation of active centers via the naturally occurring functional groups on the surface of the nanomaterials [14, 31]. However, the $MWCNT_{20–30\ nm}$ and graphene exhibited higher activity among the nanomaterials used for both S_1 and S_2 systems, respectively (Entries 4 and 8), which may be attributed to the direct adsorption of the catalysts onto the surface of the nanocarbons, and the graphene which has a higher surface to volume ratio in comparison with the other used nanomaterial [14, 31, 32].

Figure 2 exhibits the broadening of fusion area of the nano-samples prepared using S_1. The higher value of branching content for nanocomposite samples led to a shift in melting and crystallization points toward low temperatures (down to 82.0°C) and broadening as compared to those prepared by the other catalytic system [6, 33]. The highest and lowest branching contents and vinyl extent of the resulting samples using different catalytic system were, however, assigned to

Table 2. In situ polymerization results for production of nanocomposites[a]

Entry	Catalytic system	wt %[b]	Additive type	Act.[c]	T_m[d], °C	X_C[d], %	VC[e]	BD[f]	T_{deg}[g], °C
1	S_1	0	Neat	53.9	83	35.7	2.41	13.50	412, 434
2		0.74	$MWCNT_{20–30\ nm}$	28.2	82	4.0	2.77	22.36	461
3		0.80	$MWCNT_{30–50\ nm}$	26.3	82	5.2	11.35	29.92	476
4		0.30	Graphene	23.2	95	6.0	5.95	16.85	379, 434
5	S_2	0	Neat	75.6	125	20.1	0.90	32.21	440, 453
6		1.31	$MWCNT_{20–30\ nm}$	32.0	130	45.0	2.1	9.53	390, 410, 444
7		0.97	$MWCNT_{30–50\ nm}$	43.2	129	48.5	3.20	20.04	400, 454
8		0.32	Graphene	43.6	129	46.0	4.10	11.56	393, 458

[a] Conditions: toluene 100 mL, polymerization temperature 0°C, ethylene pressure 2 bars, Cat Z 5 μmol, Cat N 5 μmol (50 : 50), MMAO as co-catalyst, [Al]/[M] = 1000,
[b] wt % of nanomaterial in polymer matrix,
[c] Activity: × 10^4 g (PE) mol/(Ni+Zr) hr,
[d] Determined by DSC [26],
[e] Vinyl content: determined by FTIR [24], number of vinyl groups/1000 carbon atoms,
[f] Branching density: determined by FTIR [6], methyl branches/1000 carbon atoms,
[g] Degradation temperature: determined by TGA.

the sample produced in the presence of both $MWCNT_{30–50\ nm}$ and $MWCNT_{20–30\ nm}$ (Entries 3 and 6 and Fig. 3), respectively. Moreover, the samples obtained using S_1 showed almost similar crystallinity and melting point values than the neat polyethylene blend (Entries 1–4). In the presence of graphene, however, the melting point of the nanocomposite samples enhanced to 94.7°C, but the sample obtained using S_2 exhibited a reverse trend. The observed melting point and crystallinity percentage showed higher values than the sample produced using S_1 and neat polyethylene blends. Nevertheless, nanocomposite samples containing $MWCNT_{20–30\ nm}$ and $MWCNT_{30–50\ nm}$ indicated the highest and lowest melting temperatures in both S_2 and S_1 catalytic systems (130.4 and 82.1°C), respectively. These significant differences might be due to the high variety degree of branching as compared to the other obtained nanocomposite samples [34, 36].

Morphology of the Polyethylene Blends

Morphological study showed a uniform shape of morphology for the polyethylene blend prepared at 1 bar of the monomer pressure (Fig. 4a). However, increasing the ethylene pressure (up to 4 bar) causes two distinct phases of morphology (Fig. 4b), which can be corresponded to the separate polymerization process by each active centers in the catalyst systems (Fig. 1). Figure 4c exhibits the SEM images of polyethylene blends made by S_2. A number of polymer fibers can be indicated with various sizes and shapes, which may be ascribed to polymer extraction from micro to nanosized pores in the structure of catalysts during the polymerization [36, 37]. In fact, the catalyst structure of these fibers is made by oriented crystallization during chain propagation [38] and can be affected by elevating the ethylene pressure to high degree of crystallization, as shown in Fig. 4d (Entries 5–8, Table 2). However, with raising the reaction temperature from 0 to 20°C, this crystallization phases and sharp melting peaks disappeared and a uniform amorphous phase (rubber like) in total topology of the resulting polyethylene blend prevailed (Fig. 4e).

In Fig. 5, an almost uniform form of morphology is not seen for the resulting samples containing both $MWCNT_{20–30\ nm}$ and graphene. However, the presence of nanoparticles is evident with good dispersion in the polymer matrix (Figs. 5b–5d). For instance, an amorphous to rock sheet morphologies were observed, which was expected for $MWCNT_{20–30\ nm}$, was seen for the resulting nanocomposites in the presence of both $MWCNT_{30–50\ nm}$ and graphene.

Soft and amorphous morphologies were observed for the produced nanocomposites using S_2 catalyst system in the presence of both $MWCNT_{20–30\ nm}$ and $MWCNT_{30–50\ nm}$. It is worth to note that the samples made in the presence of MWCNTs indicated single fraction phase and higher degree of crystallinity, which can be due to good miscibility of the nanotubes in the polyethylene matrix (Fig. 6) [13].

Thermal Gravimetric Analysis (TGA)

According to our previous study, thermal stability of nanocomposites highly depends on type and content of nanoparticles [13]. The neat sample produced by first system of catalyst (S_1) showed lower thermal

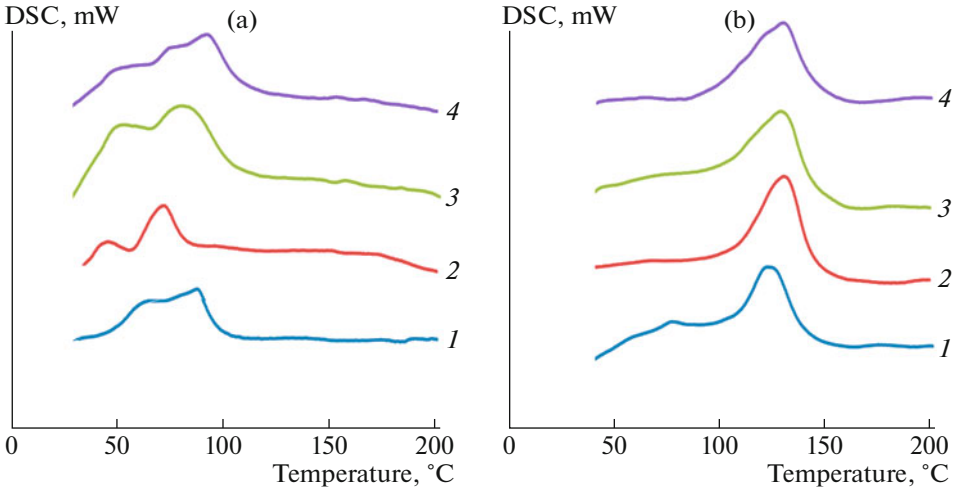

Fig. 2. DSC thermograms of (*1*) PE blend and PE/nanocomposites containing (*2*) $MWCNT_{20–30\ nm}$ (0.74 wt %), (*3*) $MWCNT_{30–50\ nm}$ (0.80 wt %), (*4*) graphene (0.30 wt %) obtained using N/Z/MMAO binary system: (a) S_1, (b) S_2.

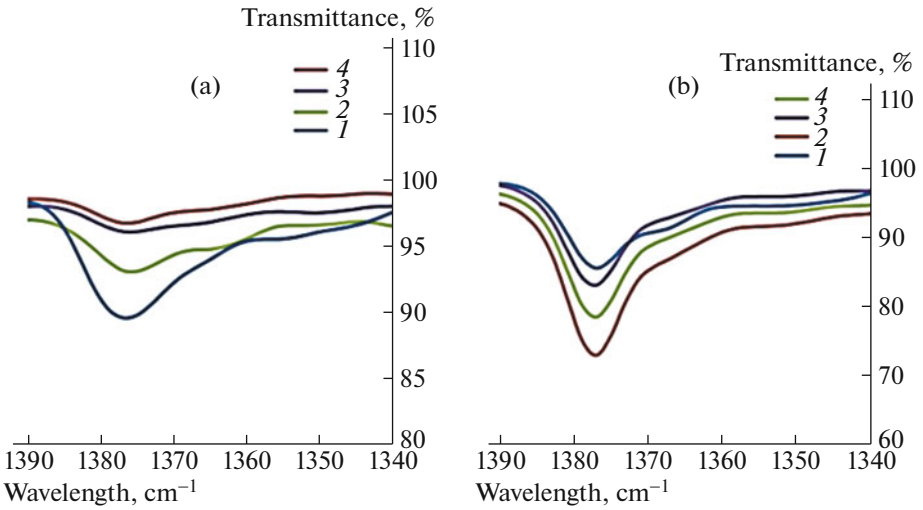

Fig. 3. FTIR spectra in the range of 1300–1400 cm^{-1} corresponding to methyl symmetrical deformation band for (*1*) the PE blend and the resultant PE/nanocomposites containing (*2*) $MWCNT_{30–50\ nm}$ (0.97 wt %), (*3*) graphene (0.32 wt %), (*4*) $MWCNT_{20–30\ nm}$ (1.31 wt %) obtained using (a) S_1; for (*1*) the PE blend and the resultant PE/nanocomposites containing (*2*) $MWCNT_{30–50\ nm}$ (0.80 wt %), (*3*) graphene (0.30 wt %), (*4*) $MWCNT_{20–30\ nm}$ (0.74 wt %) obtained using (b) S_2.

stability than its analogue produced using S_2 (Entries 1 and 5, Table 2). However, the augmentation of variety weight percent of MWCNT during the polymerization can enhance the thermal stability to higher value, while different trends were observed for the obtained samples using S_2 system (Fig. 7). This behavior can be attributed to the high influence of different catalyst system on the thermal properties of the nanocomposites. Totally, the augmentation of graphene into the polymerization media showed almost the same trend observed as the thermal degradation (Entries 4 and 8). However, the resulting nanocomposite containing of 0.32 wt % of graphene (Entry 8) exhibited better thermal stability than the analogous sample due to higher crystallinity and lower branching content [14].

CONCLUSIONS

Polymerization behavior of the catalytic combination of metallocene and synthesized complexes based on nickel was evaluated. The binary catalyst system of S_2 showed higher catalytic activity, $\bar{M}_v$ and thermal stability than the sample prepared using the zircono-

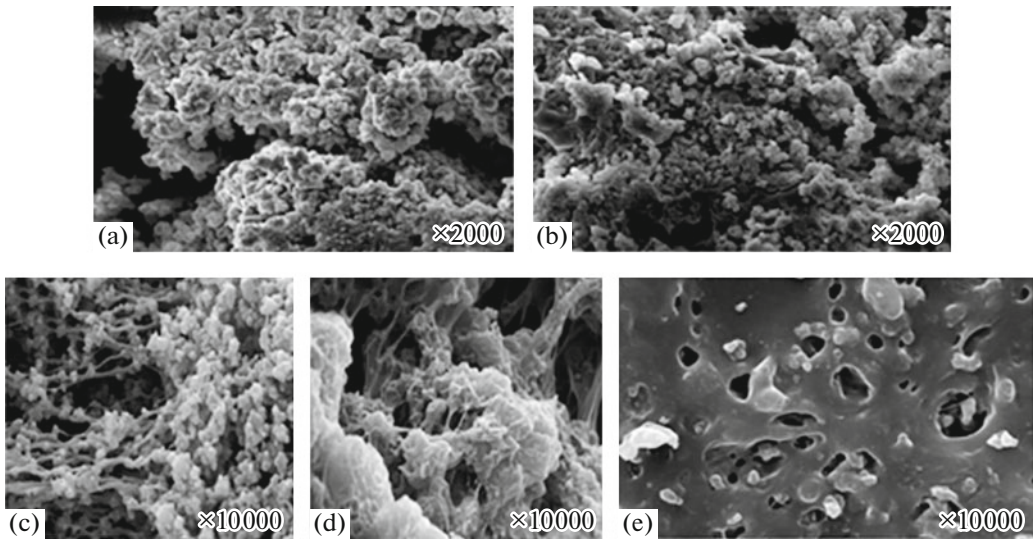

Fig. 4. SEM images of polyethylene blend prepared using N/Z/MMAO binary system of catalysts: (a) S_1 (1 bar, 0°C), (b) S_1 (4 bars, 0°C), (c) S_2 (2 bars, 0°C), (d) S_2 (4 bars, 0°C), and (e) S_2 (2 bars, 30°C).

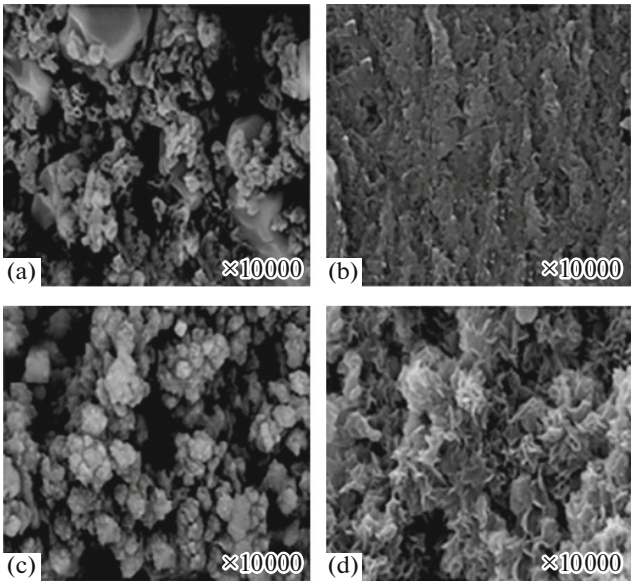

Fig. 5. SEM images of (a) polyethylene blend, and PE/nanocomposites containing (b) $MWCNT_{20-30\ nm}$ (0.74 wt %), (c) $MWCNT_{30-50\ nm}$ (0.80 wt %), (d) graphene (0.30 wt %), prepared by S_1 catalytic system.

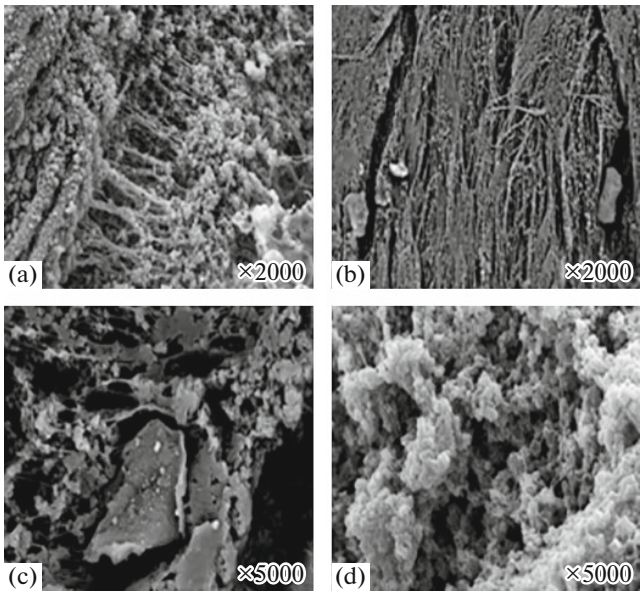

Fig. 6. SEM images of (a) polyethylene blend, and PE/nanocomposites containing (b) $MWCNT_{20-30\ nm}$ (1.31 wt %), (c) $MWCNT_{30-50\ nm}$ (0.97 wt %), (d) graphene (0.32 wt %), produced by S_2 catalytic system.

cene and pyridine-imine catalyst based on nickel (S_1). The product obtained using S_2 system demonstrated higher melting point and single distinct population of crystalline phase in both DSC traces and SEM images, which can be attributed to the lower degree of branching at the resultant reactor blends. PE/nanocomposites samples containing different types of nanomaterials were successfully prepared via in situ polymerization. However, the observed activities of both catalytic systems were reduced to about half as compared to the neat samples, and the overall performance of the resultant nanocomposites prepared by S_1 catalyst system in presence of nanomaterial was worse. The nanocomposites obtained using S_2 catalyst system showed higher melting point and distinct fibrous phase morphology that implied to lower both degree of branching and vinyl content.

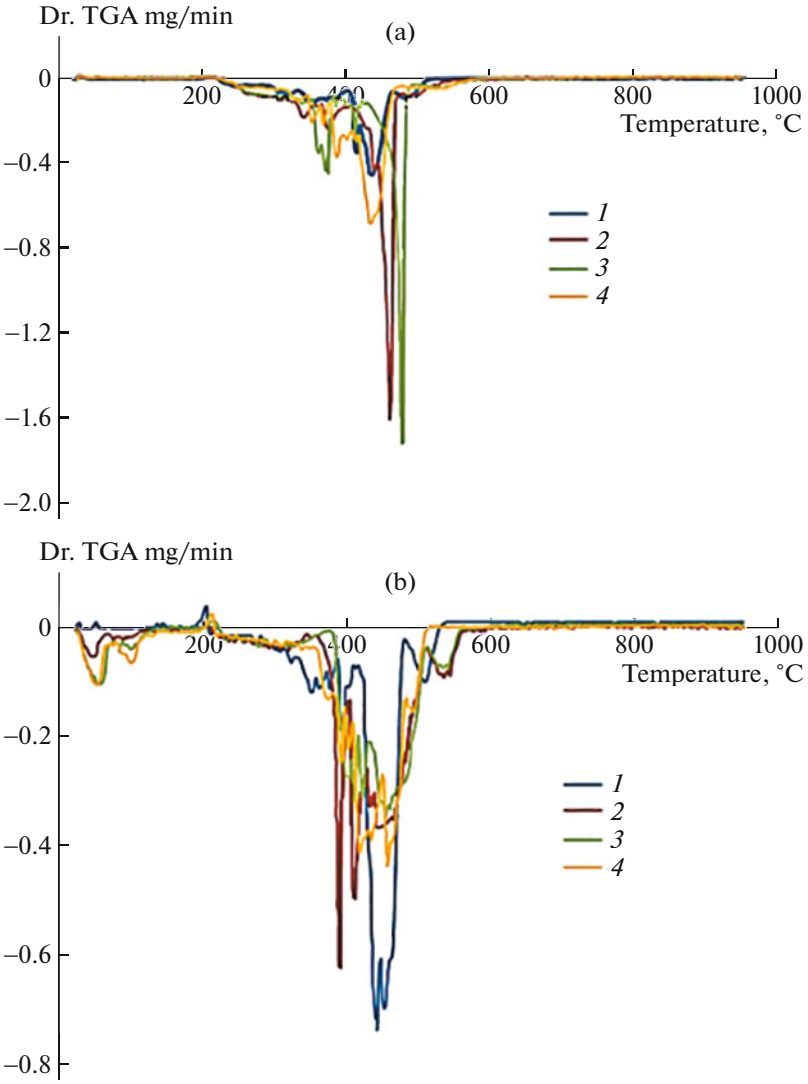

Fig. 7. Differential thermogravimetric curves of (*1*) the neat polyethylene blend and PE/nanocomposites containing (*2*) $MWCNT_{20–30\ nm}$ (0.74 wt %), (*3*) $MWCNT_{30–50\ nm}$ (0.80 wt %), (*4*) graphene (0.30 wt %) prepared by in-situ polymerization in the presence of (a) S_1; and (*1*) the neat polyethylene blend and PE/nanocomposites containing (*2*) $MWCNT_{20–30\ nm}$ (1.31 wt %), (*3*) $MWCNT_{30–50\ nm}$ (0.97 wt %), (*4*) graphene (0.32 wt %) prepared by in-situ polymerization in the presence of (b) S_2.

FUNDING

This research was financially supported by grants from Ferdowsi University of Mashhad (FUM) [grant nos. 3/44191 and 3/43962].

CONFLICT OF INTEREST

The authors declare that they have no conflict of interest.

REFERENCES

1. W. Kaminsky and M. Arndt, Adv. Polym. Sci. **127**, 143 (1997).
2. M. Delferro and T. J. Marks, Chem. Rev. **111**, 2450 (2011).
3. F. AlObaidi and S. Zhu, J. Appl. Polym. Sci. **96**, 2212 (2005).
4. C. Bianchini, M. Frediani, G. Giambastiani, W. Kaminsky, A. Meli, and E. Passaglia, Macromol. Rapid Commun. **26**, 1218 (2005).
5. W. H. Sun, S. Song, B. Li, C. Redshaw, X. Hao, Y. S. Li, and F. Wang, Dalton Trans. **41**, 11999 (2012).
6. M. Mogheiseh, G. H. Zohuri, and M. Khoshsefat, Macromol. React. Eng. **12**, 1800006 (2018).
7. C. Bianchini, G. Giambastiani, L. Luconi, and A. Meli, Coord. Chem. Rev. **254**, 431 (2010).

8. D. P. Gates, S. A. Svejda, E. Oñate, C. M. Killian, L. K. Johnson, P. S. White, and M. Brookhart, Macromolecules **33**, 2320 (2000).
9. S. D. Ittel, L. K. Johnson, and M. Brookhart, Chem. Rev. **100**, 1169 (2000).
10. R. F. De Souza and O. L. Casagrande Jr., Macromol. Rapid Commun. **22**, 1293 (2001).
11. T. O. Ahn, S. C. Hong, J. H. Kim, and D. H. Lee, J. Appl. Polym. Sci. **67**, 2213 (1998).
12. A. Lisovskii, M. Shuster, M. Gishvoliner, G. Lidor, and M. S. Eisen, J. Polym. Sci., Part A: Polym. Chem. **36**, 3063 (1998).
13. M. Mogheiseh, G. H. Zohuri, and M. Khoshsefat, J. Appl. Polym. Sci. **136**, 47376 (2019).
14. M. Khoshsefat, S. Ahmadjo, S. M. M. Mortazavi, and G. H. Zohuri, RSC Adv. **6**, 88625 (2016).
15. H. W. Park, J. S. Chung, S. S. Lim, and I. K. Song, J. Mol. Catal. A: Chem. **264**, 202 (2007).
16. M. Ahmadi, R. Jamjah, M. Nekoomanesh, G. H. Zohuri, and H. Arabi, Macromol. React. Eng. **1**, 604 (2007).
17. J. W. Suk, R. D. Piner, J. An, and R. S. Ruoff, ACS Nano **4**, 6557 (2010).
18. Z. Yin, S. Sun, T. Salim, S. Wu, X. Huang, Q. He, and H. Zhang, ACS Nano **4**, 5263 (2010).
19. S. K. Mishra, S. N. Tripathi, V. Choudhary, and B. D. Gupta, Sens. Actuators, B **199**, 190 (2014).
20. S. Park, S. W. Yoon, H. Choi, J. S. Lee, W. K. Cho, J. Kim, H. J. Park, W. S. Yun, C. H. Choi, Y. Do, and I. S. Choi, Chem. Mater. **20**, 4588 (2014).
21. A. C. Pinheiro, A. C. Casagrande, and O. L. Casagrande, Jr., J. Polym. Sci., Part A: Polym. Chem. **52**, 3506 (2014).
22. M. Khoshsefat, G. H. Zohuri, N. Ramezanian, S. Ahmadjo, and M. Haghpanah, J. Polym. Sci., Part A: Polym. Chem. **54**, 3000 (2016).
23. S. A. Sangokoya, EP Patent No. 0463555 B (1996).
24. W. Collins, J. Seelenbinder, and F. Higgins, *Determination of the Vinyl Content of Polyethylene Resins* (Agilent Technology Inc., Santa Clara, California, USA, 2012).
25. S. M. M. Mortazavi, H. Jafarian, M. Ahmadi, and S. Ahmadjo, J. Therm. Anal. Calorim. **123**, 1469 (2016).
26. S. Damavandi, N. Samadieh, S. Ahmadjo, Z. Etemadinia, and G. H. Zohuri, Eur. Polym. J. **64**, 118 (2015).
27. Z. Huang, K. Song, F. Liu, J. Long, H. Hu, H. Gao, and Q. Wu, J. Polym. Sci., Part A: Polym. Chem. **46**, 1618 (2008).
28. A. K. Tomov, V. C. Gibson, G. J. Britovsek, R. J. Long, M. van Meurs, D. J. Jones, K. P. Tellmann, and J. J. Chirinos, Organometallics **28**, 7033 (2009).
29. L. Pan, K. Y. Zhang, Y. G. Li, S. Q. Bo, and Y. S. Li, J. Appl. Polym. Sci. **104**, 4188 (2007).
30. M. Kimiaghalam, H. N. Isfahani, G. H. Zohuri, and A. Keivanloo, Appl. Organomet. Chem. **32**, e4153 (2018).
31. A. Toti, G. Giambastiani, C. Bianchini, A. Meli, S. Bredeau, P. Dubois, D. Bonduel, and M. Claes, Chem. Mater. **20**, 3092 (2008).
32. L. Vaisman, H. D. Wagner, and G. Marom, Adv. Colloid Interface Sci. **128**, 37 (2006).
33. S. Ahmadjo, S. Dehghani, G. H. Zohuri, G. R. Nejabat, H. Jafarian, M. Ahmadi, and S. M. M. Mortazavi, Macromol. React. Eng. **9**, 8 (2015).
34. L. Boggioni, G. Scalcione, A. Ravasio, F. Bertini, C. D'Arrigo, and I. Tritto, Macromol. Chem. Phys. **213**, 627 (2012).
35. L. Zhang, E. Yue, B. Liu, P. Serp, C. Redshaw, W. H. Sun, and J. Durand, J. Catal. Commun. **43**, 227 (2014).
36. Z. Ye, H. Alsyouri, S. Zhu, and Y. S. Lin, Polymer **44**, 969 (2003).
37. F. Kunrath, R. F. De Souza, and O. L. Casagrande, Jr., Macromol. Rapid Commun. **21**, 277 (2000).
38. W. Li, J. Wang, B. Jiang, Y. Yang, and Z. Jie, Polym. Int. **59**, 617 (2010).